Spectroscopic Analysis of Dwarf Ellipticals in the Fornax Cluster

F. S. Eftekhari[1,2], N. Scott[3], R. F. Peletier[1], S. Mieske[2]

1. Kapteyn Astronomical Institute, University of Groningen, The Netherlands
2. European Southern Observatory, Santiago, Chile
3. Sydney Institute for Astronomy, The University of Sydney, NSW, Australia

1. Abstract

Dwarf galaxies, being small and having low surface brightness, have not been studied well outside the Local Group. This is important, since most of our ideas about the formation and evolution of them is based on local data. Here we present deep IFU observations (R=5000) for a large sample of dEs in the Fornax Cluster, for which we study the structure, kinematics and stellar populations. Our sample includes galaxies that are 1-2 mag fainter than in other IFU surveys, allowing us to measure velocity dispersions down to 10 km/s. In this poster we present the angular momentum distribution, showing that dwarfs rotate much less than giant galaxies. We see that dwarfs follow the same Fundamental Plane and Faber Jackson relation as giant galaxies. Also the observed local DM fraction of cluster galaxies is the same as in the local group.

2. Scientific Qs.

Do dEs and giant galaxies follow the same scaling relations?(FP, FJ, etc.)
What is the DM contents of faint cluster dEs?
What is the physical role of the environment in the evolution of dEs?
What is the fraction of rotational over pressure supported dEs?
FUTURE WORK
Can we detect the effects of starvation or ram-pressure on dEs?
How do the stellar populations of dEs depend on the environment ?

3. Analysis

We extracted stellar kinematics and stellar populations from the absorption-line spectra of our galaxies by using the penalised Pixel Fitting (pPXF) routine of Cappellari & Emsellen (2004). pPXF basically is a maximum penalized likelihood approach in pixel space, with the aim of finding an optimal temple with the minimum template-galaxy mismatch errors. It finds the best-fitting linear combination of input stellar templates by convolving them with the line-of-sight velocity distribution of the input galaxy's spectra, and then the best-fitting parameters are determined by a non-linear chi-squared minimization in pixel space (logarithmically binned in wavelength).
Moreover, we computed the uncertainties by (100 realizations) Monte Carlo simulations. In each loop the best-fitted spectrum is disturbed by random spectra convolved by the sigma of the difference between original and best-fitted template spectra. The best match for the SAMI-Fornax's wavelength range and spectral resolution is single-age single-metallicity population models of PEGASE-HR (Le Borgne et al. 2004). ELODIE is a high resolution stellar library of 1959 spectra for 1503 stars with R=10 000 at lambda=550 nm.

4. Sample & Data

The SAMI Fornax project started in 2015 with the Sydney-AAO Multi-Object Integral-field (SAMI) spectrograph on the Anglo-Australian Telescope (AAT), with the aim of studying the origin and the inner processes of dwarf galaxies inside the Fornax cluster. We performed deep observations of 5-7 hours exposure time, observing 12 galaxies at the same time, during 3 observing runs in 2015B, 2016B and 2018B, resulting in 37 dwarf galaxies and 14 giant elliptical galaxies with spectra allowing us to measure stellar kinematics.
SAMI is an integral-field spectrograph equipped with 13 fiber-based IFUs called hexabundles, and 26 pluggable sky fibers (Bryant et al. 2014). Each hexabundle with a field-of-view of 15" diameter, is made of 61 1.6" optical fibers. These hexabundles have physical size <1 mm, with a filling fraction of 73% and together with the sky fibers each fits into pre-drilled holes in a field plate. The plug plate with about one degree field-of-view is installed at the AAT's Prime Focus Camera top end placing the face of hexabundle at the focal plane of the telescope.
To study the structure of low-mass galaxies such as dEs in the Fornax cluster, high resolution spectra and high S/N are needed. With the 1500V gratings in the blue and the 100R gratings in the red, our data has a resolution of ~5100 (FWHM = 1.0Å) in the blue ($\sim 4660 - 5430$Å) and ~4300 (FWHM = 1.6Å) in the red ($6250 - 7350$Å). This means that we can potentially reach velocity dispersion of about 10 km/s in both blue and red.

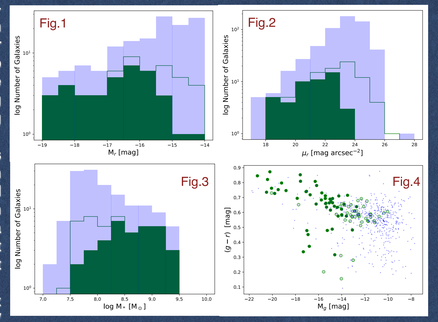

(Fig. 4) The M_g vs colour-magnitude diagram for our sample (green circles), compared to that from the full FDS sample (blue crosses). We primarily target galaxies on the red sequence, but do include some blue galaxies that satisfy our selection criteria.

Our sample was selected based on the Fornax Deep Survey (FDS, Venhola et al. 2019). Considering that the aim was to study star formation and evolution of dEs within the Fornax cluster, the primary survey targets are FDS galaxies that cover the range $-18 < M_r < -14.5$ and $17 < \mu_r < 23$, in environments ranging from the center of the cluster to positions outside of its virial radius (4° or 1.4 Mpc) such as dEs in the Fornax A region.
(Fig. 1, 2& 3) These figures show that our sample is representative of the dwarfs in the Fornax Cluster. We show the number of galaxies as a function of surface brightness, absolute magnitude and stellar mass. The open green histogram shows the distribution for all observed SAMI-Fornax galaxies, while the solid green histogram indicates only those for which we were successful in measuring stellar kinematics. The pale blue histogram indicates the distribution for the full FDS sample.

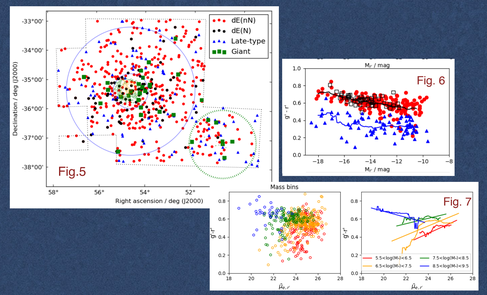

(Fig. 5) Spatial coverage of the FDS, indicating the main cluster with its virial radius together with the infalling group towards the South West, centered around NGC 1316 (Fornax A). Indicated are the galaxy members (excluding UCDs): giants from Iodice et al. (2019) and dwarfs from Venhola et al. (2019).
(Fig. 6) Color-magnitude diagram of dwarfs in the FDS. From Venhola et al. (2019).
(Fig. 7) Color vs. surface brightness for Fornax dwarfs. The left panel shows the relation for the individual galaxies, and the right panels show the running medians and linear fits for the different bins.

Fornax Deep Survey

The Fornax Deep Survey (Iodice et al. 2016, Venhola et al. 2018) is an ultradeep survey of 30 square degrees of the Fornax Cluster, observed with ESO's VST using OMEGACAM. Its imaging is approximately as deep as the NGVS (Ferrarese et al. 2012). With integration times of 11000 s in u, 8000 s in g, 8000 s in r, and 5000 s in i, we are reaching a surface brightness at S/N=1 per arcsec-2 of 28.0 mag arcsec-2 in u, 28.6 in g, 28.1 in r, and 27.2 in i. In Venhola et al. (2018) a complete sample of dwarf galaxies is defined, superseding the old Fornax Cluster Catalog (Ferguson 1989) (Fig. 5). Its photometric properties are described in Venhola et al. (2019). FDS has been used for several applications related to the stellar halos of massive ellipticals in Fornax, globular clusters, CO-gas in dwarfs (Zabel et al. 2019), and HI in the Fornax A group (Serra et al. 2019) using MeerKAT. We are currently making the reduced images available through the ESO Science Archive.
The photometric analysis of FDS has given us some clues about the physical processes that are active when a gas-rich dwarf falls into the cluster. The dwarfs form reasonably tight color-magnitude diagrams (e.g. Fig. 6), with a distinct fraction, growing towards fainter galaxies, showing signs of star formation, and therefore classified as irregular dwarfs. The color-magnitude diagrams agree with those in Virgo, with the fraction of irrgulars increasing towards the outer parts of the cluster. Interesting is the relation between color and surface brightness (Fig. 7). While for most galaxies redder galaxies have lower surface brightness, something which happens when galaxies are fading when they age, we see the opposite for the brightest dwarfs. Here the reddest objects have the highest surface brightness. We think (Venhola et al. 2019) that in those objects galaxy harassment is taking place, removing the outer layers of the dwarfs and making them redder for their remaining mass, while the fainter dwarfs end up on a fading sequence, after having lost most of their gas due to ram pressure stripping.

5. Preliminary Science Results

1. Angular-Momentum

From our maps of stellar velocity and stellar velocity dispersion we measure λ_R, the specific stellar angular momentum, a proxy for the degree of rotational or pressure support within a galaxy. In the left figure we show profiles of λ_R vs r/R_e for galaxies of different stellar mass. For massive galaxies our radial coverage is limited, however for low mass galaxies we can trace the angular momentum out to relatively large radii. These profiles show a variety of behaviour – either rising rapidly then flattening at large radius or staying low at all radii. In the right hand figure we show the distribution of our galaxies in the λ_R - ellipticity plane. Galaxies below a $\lambda_R \sim 0.1$are classified as slow rotators, systems with very low specific stellar angular momentum, often indicative of an evolutionary history involving significant dynamical interactions such as merging or harassment.

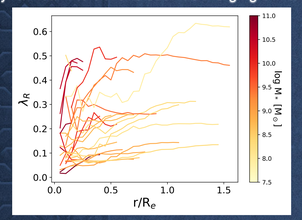

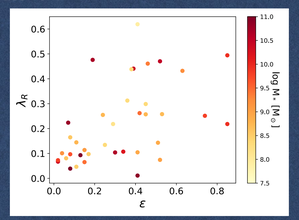

2. Faber-Jackson Relation

One of the first discoveries in early-type galaxies was that their stellar velocity dispersion correlates with their luminosity (Faber & Jackson 1967). This two dimensional relation $L \sim \sigma^{\alpha}$ Faber-Jackson relation is in fact a projection of the Fundamental Plane.
We see the same slope from giants to dwarf ellipticals, and so they seem to have same internal structure. As we go to fainter objects we continue to have tight relation.

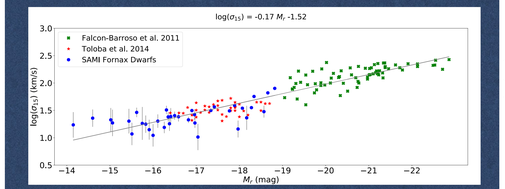

3. Fundamental Plane

The empirical Fundamental plane which is a bivariate relation (Brosche 1973, Dressler et al. 1973 and Djorgovski & Davis 1987) between R_e(the half light ration radius of the galaxy), I_e (the mean surface brightness within R_e in flux units), and σ (the galaxy internal velocity dispersion), is an indication of galaxies being in Virial equilibrium $R_e \propto \sigma^2 I_e^{-1}(M/L)^{-1}$ (Binney & Tremaine 2008).
We find that all of the objects are in Virial equilibrium, and again dEs and Es follow the same slope. The upturn of dEs in the faintest region might be only due to selection effect, since the S/N of galaxies with lower dispersions could be too low to measure kinematics on.

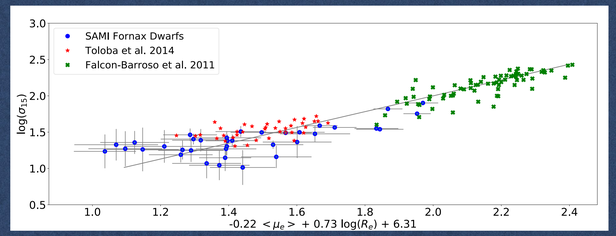

4. Dynamical Mass vs. Stellar Mass

Not considering the difference between radial and tangential velocity dispersion weakens our ability to reach accurate conclusions about the structure and formations of galaxies. This becomes more important in calculating dynamical mass of a galaxy by only having its 2d observed radial properties. Wolf et al. (2010) showed that within r_3 radius (where the log-slope of the 3D tracer density profile is -3) this difference is insignificant.
Also similar to Venhola et al. 2019 we estimate the stellar mass of the sample galaxies using the empirical relation observed between the g'-i' color and the mass-to light (M/L) ratio using prescription of Taylor et al. (2011).

We find that our galaxies connect well with the brighter dwarfs from Toloba et al (2014), and the Local Group dwarfs from Wolf et al (2010). This means that the dark matter properties of these dwarfs in clusters are the same as in the Local Group, implying that the dark matter distribution inside the galaxies is not affected by the cluster environment.

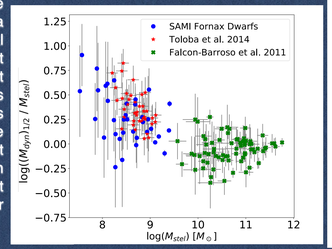

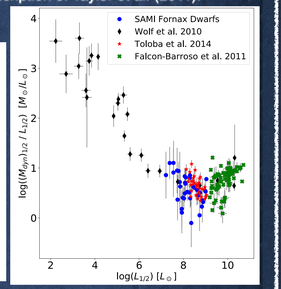

5. Kinematic Maps

The velocity and velocity dispersion maps of 5 representative SAMI-Fornax galaxies. The photometric images are taken from the FDS catalog. The red circle is the field-of-view of SAMI, which is 15" diameter.

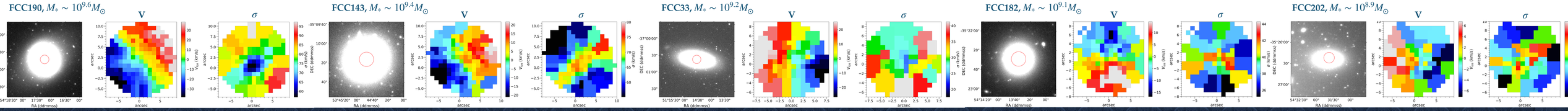

References

Bryant J. J., et al., 2015, MNRAS, 447, 2857
Brosche, P. 1973, A&A, 23, 259
Cappellari M., Emsellem E., 2004, Publ. Astron. Soc. Pacific, 116, 138
Djorgovski S., Davis M., 1987, ApJ, 313, 59
Dressler A., et al., 1987, ApJ, 313, 42
Faber S. M., Jackson R. E., 1976, ApJ, 204, 668
Ferguson, H., 1989, AJ, 98, 367
Ferrarese, L., et al., 2012, ApJS, 200, 4
Falcon-Barroso, J., et al. 2011b, MNRAS, 417, 1787
Iodice, E., et al., 2016, ApJ, 820, 42
Iodice, E., et al., 2019, A&A, 623, 1
Le Borgne D., et al., 2004, A&A, 425, 881
Serra, P., et al., 2019, arXiv: 1905.08265, A&A, in press
Taylor E. N., et al., et al. 2011, MNRAS, 418, 1587
Toloba E., et al., 2014a, ApJS, 215, 17
Venhola, A., et al. 2017, A&A, 608, A142
Wolf, J., et al., 2010, MNRAS, 406, 1220
Zabel, N., et al., 2019, MNRAS, 483, 2251